FULLY PLASTIC *J*-INTEGRALS FOR MIXED MODE FRACTURE INDUCED BY INCLINED SURFACE CRACKS IN PRESSURIZED DUCTILE PIPES

Weigang Wang[1], Wei Yang[2] and Chun-Qing Li[1,*]

[1]School of Engineering, RMIT University, Melbourne, 3001, Australia
[2]Faculty of Architecture, Building and Planning, The University of Melbourne, Australia

ABSTRACT

Surface cracks have been recognized as major causes for fracture failures of ductile pipes. This paper intends to derive a normalized fully plastic *J*-integral solution to mixed-mode fracture caused by inclined surface cracks in pressurized ductile pipes. A combined *J*-integral and finite element method is developed to evaluate the *J*-integral for inclined surface cracks. A set of predictive formulas for normalized fully plastic *J*-integrals are developed. It is found in this paper that the normalized fully plastic *J*-integral increases with the decrease of crack inclination angle and aspect ratios, and the increase of strain hardening exponent. It is also found that the critical locations of crack propagation occur between the surface point and the deepest point of cracks when the inclination angle is relatively small. The paper concludes that the developed formulas can accurately predict the normalized fully plastic *J*-integrals along the front of inclined surface cracks. The results presented in the paper can enable researchers and practitioners to accurately predict the mixed-mode fracture failure of pressurized pipes subject to inclined surface cracks.

KEYWORDS

Inclined surface crack; Mixed-mode fracture; *J*-integral; Thin-wall pipes; Internal pressure

[*]*Corresponding author, Professor Chun-Qing Li, email: chunqing.li@rmit.edu.au*

INTRODUCTION

Ductile pipes are widely used in the transmission and distribution of water, oil and gas. During their service life, these metal pipes are susceptible to pitting corrosion, which can induce surface cracks in the pipes (Conlin and Baker 1991). Under the service loading, the cracked pipes can easily fail due to the intensified stresses at the crack tip. Thus, surface cracks have been recognized as a major cause of pipe failures. To prevent catastrophic failures of pipes, it is imperative to accurately determine the fracture resistance of cracked pipes and identify those affecting factors.

Considerable research has been undertaken to understand the fracture resistance of cracked cylindrical structures and to determine their *J*-integrals for various surface cracks. For example, Parks and White (1982) developed a method for estimating *J*-integrals for internally pressurized cylinders subject to a longitudinal part-through surface crack by use of both the virtual crack extension method and line-spring finite element models. Kumar and German (1988) and Kumar et al. (1981) determined the *J*-integrals for cylinders with longitudinal and circumferential cracks by use of two dimensional (2D) finite element models in which the three-dimensional (3D) problems were assumed to be either a plane strain or axisymmetric condition. Jayadevan et al. (2004) and Østby et al. (2005) investigated the effects of geometries and material properties on the crack tip opening displacement of circumferentially cracked offshore pipelines under pure tensile loading as well as tension with internal pressure by use of a detailed 3D elastic–plastic finite element method. Cho et al. (2011) derived new normalized fully plastic *J*-integral solutions for pipes with circumferential semi-elliptical surface cracks for a wide range of geometries, material properties and loading conditions (tension, bending and internal pressure) based on extensive finite element simulations. Liu et

al. (2018) conducted similar finite element analyses to determine the *J*-integrals for welded thin-wall steel pipes with constant-depth circumferential surface cracks.

All the above investigations for cracked pipes are either for longitudinal or circumferential cracks and only the single fracture mode was considered. However, the initial orientation of crack has been found to vary widely and most likely as inclined cracks (Shlyannikov 2013). There are many factors, e.g., anisotropic residual stresses and corrosion ptis (Zadow et al. 2015), complex loading conditions and welding methods (Aliha and Ayatollahi 2007), that contribute to inclined surface cracks. A systematic survey of exhumed X65 gas pipelines in Australia by Zadow et al. (2015) shows that 81% of cracks grow away from either the longitudinal or the circumferential direction, i.e., they are inclined. These inclined surfaces cracks can often induce spiral fractures in pressurized pipes (National Research Council 2006, Makar et al. 2001) which is more likely to be mixed-mode rather than single-mode. Although some researchers, e.g., Shahani and Habibi (2007) and Moghaddam et al. (2013), and Li et al. (2016), determined the stress intensity factors for cracked cylinders under the mixed-mode conditions, the results are only valid for elastic materials and ductile materials under small scale yielding conditions. For pipes made of elasto-plastic materials, e.g., ductile iron and steel pipes, a more rational and accurate approach for investigating their fracture resistance is to determine the elastic-plastic fracture parameters, e.g., *J*-integral.

A thorough review of literature shows that very few studies have been undertaken on the mixed-mode fracture of steel pipes (and even fewer for ductile iron) induced by inclined surface cracks. There is still a lack of *J*-integrals solutions for pressurized ductile pipes, e.g., ductile iron and steel pipes, subject to inclined surface cracks. Fu et al. (2017) is one of few researchers who determine the *J*-integrals for inclined surface cracks induced mixed-mode fracture by employing the detailed three-dimensional finite element method. However, that

74 study was limited to finite-thickness plates but not for pipes. More recently, Wang et al.
75 (2020) determined the elasto-plastic *J*-integrals of pressurized steel pipes but the geometry of
76 crack is only limited to longitudinal cracks and only Mode I fracture was considered.
77 Furthermore, there is lack of predictive models of elasto-plastic *J*-integrals for ductile pipes
78 with inclined surface cracks and lack of explicit investigation on the effects of crack
79 geometries and material properties on elasto-plastic *J*-integrals. Considering the important
80 role of ductile pipes in a nation's economy, environment and public well-being, there is a
81 well-justified need to thoroughly investigate their fracture resistance under mixed-mode
82 loading conditions.

83 This paper intends to determine the fully plastic *J*-integrals and develop their predictive
84 models for pressurized ductile pipes subjected to inclined surface cracks. In this paper, a
85 combined *J*-integral and three-dimensional finite element (3D FE) method is developed to
86 determine fully plastic *J*-integrals for inclined cracks. The deformation theory of plasticity is
87 used to simplify the parametric evaluations of *J*-integrals for pipes subject to inclined cracks.
88 After verification of the developed FE models, the effects of crack inclination angles,
89 material properties, crack geometries (crack depth, aspect ratio, etc.) and pipe dimensions on
90 the fully plastic *J*-integrals for pressurized pipes are thoroughly investigated. The predictive
91 formulas for both the maximum fully plastic *J*-integral and those at different locations of the
92 crack front are developed with Evolutionary Polynomial Regression (EPR) method.

93 The innovation of the presented research is not only that new solutions to *J*-integral for
94 ductile pipes with inclined surface cracks are derived but also that predictive formulas are
95 developed that cover a wide range of geometry and material properties for practical
96 applications. Furthermore, a new criterion for extracting the plastic *J*-integral is proposed in
97 the paper and the influence of geometric and material properties on the normalized fully

plastic J-integrals is thoroughly investigated. The results presented in the paper provide a useful tool for failure assessment of ductile pipes with mixed-mode fracture.

INCLINED SURFACE CRACKS IN PIPES

Surface cracks in pipes are often assumed to be of semi-elliptical shape. In FE analysis, the inclined cracks need to be expressed analytically. To achieve this, the inclined cracks can be formed by placing the centre of an elliptical crack plane at the external surface of the pipe and rotating its plane around the pipe axis with an angle of β. The actual shape of an inclined crack is the overlapped area of the crack ellipse and the curved pipe external surface as shown in Figure 1.

Figure 1 Schematic of a pipe subject to an inclined external surface crack

Mathematically, let the origin of the Cartesian coordinate system be located at the centre of the elliptical crack plane. The semi-major axis of the crack ellipse is assumed to be the x-axis while its semi-minor axis is y-axis. The crack depth, length and outer radius of the pipe are a, $2c$ and R_o, respectively. φ is the eccentric anomaly of the crack ellipse, and φ_1 and φ_2 represent the two intersection points of the crack plane and the external surface of the pipe. l_c is defined as the half arc-length of the crack front. The equation of a crack ellipse can be expressed analytically as follows

$$\begin{cases} x = c\cos\varphi \\ y = a\sin\varphi \end{cases} \tag{1}$$

The outer profile of the inclined pipe section in which the crack ellipse is placed can be also expressed as follows

$$\begin{cases} x = \dfrac{R_o}{\sin\beta}\cos\gamma \\ y = R_o \sin\gamma - R_o \end{cases} \tag{2}$$

where γ is the eccentric anomaly of pipe section outer curve which ranges from 0 to 2π. Solving Equations (1) and (2) simultaneously, the intersection of the two curves can be determined as follows

$$\varphi_{1,2} = \arcsin\left(\left(-0.5\,a\,R_o \pm \sqrt{{R_o}^2 a^2 - a^2 c^2 \sin^2\beta - a^4 \sin^4\beta}\right)/\left(a^2 - c^2\sin^2\beta\right)\right) \tag{3}$$

The half arc-length of the crack front can be calculated through the elliptic integral of the second kind as follows

$$l_c = \frac{a}{2}\int_{\varphi_2}^{\varphi_1} \sqrt{1-\left(1-a^2/c^2\right) sin^2\varphi}\, d\varphi \tag{4}$$

In a developed FE model, the position of an arbitrary point P at the crack front can be expressed as follows

$$\xi_P = \frac{l_P(\varphi)}{l_c}\left(\varphi_2 \le \varphi \le \varphi_1\right) \tag{5}$$

where $l_P(\varphi)$ is the length of the arc between the point P and the deepest point of crack.

J-INTEGRAL FOR ELASTO-PLASTIC MATERIALS

J-integral physically represents the change of the total potential energy associated with a virtual crack extension (Standard ASTM 2001). Rice and Rosengren (1968) showed that *J*-integral uniquely characterizes crack tip stresses and strains in nonlinear materials. So far, *J*-integrals have been used successfully in characterizing crack tip behavior for nonlinear materials. Mathematically, *J*-integral can be expressed as follows

$$J = \lim \int_{\Gamma} \left(\sigma_{ij} u_{j,1} - W \delta_{1i} \right) m_i \, d\Gamma \tag{6}$$

where σ_{ij} and $u_{j,1}$ are the stress and displacement components, respectively. $u_{j,1} = \frac{\partial u_j}{\partial x_1}$, W is the elastic strain energy density, $\delta_{1i}$is the Kronecker delta function, Γ is a contour that encloses the crack tip and $m_i$is the unit vector perpendicular to the contourΓ.

For ductile materials, the elasto-plastic J-integral consists of the elastic and plastic portions expressed as follows

$$J = J_e + J_P \tag{7}$$

where J_e and J_P represent the elastic and fully plastic J-integral, respectively.

The elastic J-integral equals to the energy release rate (G) which can be related to mixed-mode stress intensity factors KI, KII, and KIII, corresponding to three types of fracture modes as follows

$$J_e = G = \frac{K_I^2}{E'} + \frac{K_{II}^2}{E'} + \frac{(1+\nu) K_{III}^2}{E} \tag{8}$$

In this study, the interaction integral method is used to extract these three stress intensity factors as follows (Fu et al. 2017)

$$\begin{Bmatrix} K_{\mathrm{I}} \\ K_{\mathrm{II}} \\ K_{\mathrm{III}} \end{Bmatrix} = 4\pi \begin{Bmatrix} B_{11} & ¿ \\ B_{22} & ¿ B_{33} \end{Bmatrix} ¿ \tag{9}$$

where $B_{11}=B_{22}=G/(4\pi-4\pi\nu)$, $B_{33}=G/4\pi$, $J_{\int ¿^{I} ¿}$, $J_{\int ¿^{II} ¿}$ and $J_{\int ¿^{III} ¿}$ are the interaction *J*-integrals corresponding to auxiliary Mode I, II and III, respectively, which can be determined through 3D FE simulations.

To derive the solutions of fully plastic *J*-integral, the Ramberg-Osgood (R-O) material model, which is based on the deformation theory of plasticity, is used. The stress-strain law for R-O material can be written as follows

$$\frac{\varepsilon}{\varepsilon_o}=\frac{\sigma}{\sigma_o}+\alpha\left(\frac{\sigma}{\sigma_o}\right)^n \tag{10}$$

where α is a material constant, n is the strain hardening exponent, $\sigma_o$is the reference stress usually taken as the yield stress and$\varepsilon_o=\sigma_o/E$. The deformation theory of plasticity and incremental plasticity are essentially analogous when the applied loads increase proportionally and monotonically.

The plastic portion of *J*-integral can be expressed as follows (Lei 2004, Kumar et al. 1981)

$$J_P=\alpha\,\varepsilon_o\sigma_o L\frac{a}{d}h\left(\frac{a}{d},\frac{a}{c},\frac{d}{R},\varphi,\beta\right)\left(\frac{\sigma^{\infty}}{\sigma_o}\right)^{n+1} \tag{11}$$

where h is called the normalized fully plastic *J*-integral, which is a dimensionless function of geometry and material properties, L is a characteristic length for the cracked body which can be defined arbitrarily, c is the half-length of the crack, d is the pipe wall thickness and R is the mean radius of the pipe.

Therefore, the normalized fully plastic *J*-integral can be determined from Equation (11) by excluding the J_e from the total *J*-integral as follows

$$h\left(\frac{a}{d},\frac{a}{c},\frac{d}{R},\varphi,\beta\right)=\frac{J-J_e}{\alpha\,\varepsilon_o\sigma_o L}\frac{d}{a}\left(\frac{\sigma^{\infty}}{\sigma_o}\right)^{-n-1} \quad (12)$$

It is well known that numerical approaches based on the finite element method have reasonable accuracy in determining *J*-integral for a cracked body (Li and Yang 2012, Østby et al. 2005, Anderson 2005, Raju and Newman 1979, 1981 and 1982). In the present study, the finite element software ABAQUS (ABAQUS 2014) is employed for stress and strain analysis where various three-dimensional finite element models for cracked pipes are developed.

THREE-DIMENSIONAL FINITE ELEMENT MODELING

To derive the *J*-integrals of pressurized ductile pipes subject to inclined surface cracks with various geometries and material properties, a series of detailed 3D finite element models need to be constructed. In terms of geometries of FE models, the pipe length (l) was taken to be long enough compared to the size of the crack, i.e., $l \geq 40c$, to reduce the effects of the boundary. Two pipe wall thickness to inner radius ratios were chosen as d/R_i =0.1, 0.025, which correspond to the thick-wall and thin-wall pipes, respectively. The pressure was directly applied to the inner surface of the pipe which was restricted at the bottom to prohibit its rigid rotation. No assumption is needed concerning the state of stress since the calculations are based on detailed 3D finite element analysis. In the proposed FE model, the aspect ratios of crack (a/c) are 0.4, 1.0 and 1.5 (from low to high aspect ratios), and the relative depth ratios (a/d) are 0.2, 0.5 and 0.8 (from shallow to deep cracks). An examination on cracks by Gamboa et al. (2008) shows that the inclination angle of most surface cracks tends to be between 30° and 60°. In this paper, the inclination angle (β) is taken as 15°, 45°, and 75° to cover this range.

For material properties, the Ramberg-Osgood material model is used, the parameters of which need to be determined from stress-strain curves obtained from uniaxial tensile tests. In the present study, R-O model fitting is first performed on ductile metals, such as commonly used ductile irons (sourced from Aristizabal et al. 2011) and low carbon steels (e.g., Australian G350), as shown in Figure 2. Overall, R-O fitting works satisfactorily for both ductile iron and steels. In particular, it fits well with materials without significant plateau, e.g., ductile iron, on the stress-strain curve. In general, the strain hardening exponents obtained from R-O fittings are less then 10. Therefore, the strain hardening exponents (n) of 3, 5 and 10 are considered in this study. This strain hardening exponent range also covers the commonly used API 5L X60 to X65 steels as noted in Liu et al. (2018). Since the normalized fully plastic J-integral is independent of other material parameters (Kumar et al. 1981), they were assumed as follows for the purpose of simplification and consistency; namely, Poisson's ratio ν = 0.3, Young's modulus E= 207 GPa, yield stress σ_o= 210 MPa and material constant $\alpha = 1$. In total, 162 FE models were developed to consider various properties of geometry of crack, pipe and material.

Figure 2 R-O fitting for stress-strain curves of ductile iron (Aristizabal et al. 2011) and Australian steel G350.

Figure 3 shows a typical finite element mesh for a pipe with d/R= 0.025 and β= 45°. The domain integral method (Nikishkov and Atluri 1987) was used to evaluate the total J-integral and the elastic J-integral (the interaction energy release rates $J_{\int ¿^1}, J_{\int ¿^2, J_{\int ¿^3}, ¿}$). To do this, a crack tunnel was constructed by use of second-order singular elements as proposed by Barsoum (1975), which includes the first block of elements meshed with focused 15-node wedges elements (C3D15) and the rest of rings meshed with 20-node hexahedron elements with reduced integration points (C3D20R) as shown in Figure 3b. The first five rings of elements

except for its first block were used for evaluating the *J*-integrals. To ensure the accuracy of the *J*-integral, the crack-tip strain singularities were considered. To be more specific, the nodes at the crack tip were tied during the evaluation of elastic *J*-integral and the elements were modified by shifting the mid-side nodes to one-quarter of element edge length to archive a strain singularity of $1/\sqrt{r}$. The crack-tip nodes, at the elasto-plastic analysis, were set free independently and the crack-tip strain singularity was taken to be $r^{-1/(n+1)}$ for power-law materials (Sih and Lee 1989).

Figure 3 Finite element model of a pressurized pipe subject to an inclined surface crack

After proper partition of the pipe geometry around the inclined surface crack, the 10-node quadratic tetrahedron elements (C3D10) were applied at the irregular region of the model and the other parts were modelled by the 20-node hexahedron elements with reduced integration points (C3D20R). The tie constraints were applied to the interfaces of regions with different types of elements. To model the inclined surface crack located at the external surface of the pipe, the overlapping duplicate nodes were assigned at the element edges which constitute the surface of the crack. This defines two faces lying on top of one another but can separate during the fracture analysis. Also, mesh convergence tests were carried out to obtain the desired mesh size and a fine mesh was especially applied at the domain integral zone as seen in Figure 3c and 3d to further improve the accuracy of the *J*-integral when the material becomes highly nonlinear.

MODEL VERIFICATION

Before calculating the *J*-integral for cracked pipes, it is essential to verify the accuracy of the proposed 3D FE models. Two verifications are conducted in this paper for determining the

elastic part (stress intensity factors) and plastic part of mixed-mode elasto-plastic *J*-integral, respectively.

One is an embedded inclined circular crack in an infinite body under far-field tension load (Ayhan 2004) as shown in Figure 4a. In this paper, the 3D finite element was constructed as a cylindrical rod with a radius of R and an inclined circular crack at its centre. The length of the FE model was taken to be more than 20 times of the crack depth to reduce the boundary effects. The same crack size (a/R=0.1) and inclination angle (β=30^o) as that in Ayhan (2004) were used. Due to the symmetry, only half of the cylindrical rod was modeled. The comparison of present results and Ayhan's results, in form of normalized stress intensity factors ($K_I/\sigma\sqrt{a}, K_{II}/\sigma\sqrt{a}, K_{III}/\sigma\sqrt{a}$), is presented in Figure 5a. It can be seen from the results that, in general, good agreement is achieved between the present results and that of and Ayhan (2004) with the maximum error less than 1%.

Figure 4 (a) Schematic diagram and FE model for an infinite body with an inclined crack under tension loading, and (b) comparison of the present finite element results with Ayhan (2004).

The second verification case is a plate with an inclined crack under biaxial loading (Fu et al. 2017), as shown in Figure 5a. The width and height of the plate were set sufficiently large to reduce the boundary effects. A biaxiality ratio, defined as the ratio of the stress along the y-axis (global coordinate system of FE model) to the stress along its x-axis, of was chosen as 1.0. One-half of FE model can be seen in Figure 5a. For extracting the plastic portion of total *J*-integral, the method of Wang (2006) was adopted, that is accounting for more than 95% of the total *J*-integral for all points along a crack front. The characteristic length L (in Equation 11) is taken as the plate thickness d. The results determined by the proposed FE models are then compared to that of Fu et al. (2017). A typical comparison with a crack of a/d = 0.2 and

0.5, and n=3 and 5 is shown in Figure 5b. The comparison shows a result of average error being -1.59% with a maximum difference of only 3.1%, which suggests that the fully plastic J-integrals obtained from the proposed FE model are accurate and reliable.

Figure 5 (a) Schematic diagram and FE model for a plate with an inclined crack under biaxial loading, and (b) comparison of the present finite element results with Fu et al. (2017).

DETERMINATION OF NORMALIZED FULLY PLASTIC *J*-INTEGRAL

After the FE models verified, the normalized fully plastic J-integral (h) along the crack front line can be determined. It is well known that h largely depends on the applied load when applied loads are relatively small (Kim et al. 2004). To determine the fully plastic conditions for a cracked body, Wang (2006) proposed a criterion that the fully plastic J-integral component accounts for 95% of the total J-integral for all points of a crack. In this paper, its efficiency was re-analyzed for cracked pipes with different material properties. To be specific, different loads (internal pressure) were applied to the cracked pipes and the plastic J-integrals are extracted and then compared against its total J-integral. A typical plot of the ratio of plastic J-integral to the total J-integral (J_p/J) against h is presented in Figure 6. The results confirm that with the increase of applied load or J_p/J, the dependence of h on the load gradually decreases. However, it is also found from the present studies that the difference of h between $J_p/J\%=95\%$ and $J_p/J\%=99\%$ can be larger than 3.5% for pipes with strain hardening exponent n=5 and 10. Theoretically, using a criterion with the value of $J_p/J\%$ being 100% produces the most results of fully plastic J-integrals. A further observation from Figure 6 shows that the use of $J_p/J\%$=98% as the extraction criterion can reduce the difference from 3.5 %, as used in Wang (2006), to less than 1%. Therefore, in this paper,

Wang's (2006) criterion is modified from $J_p/J\%=¿95\%$ to $J_p/J\%=¿98\%$ to obtain h more closely representing the fully plastic J-integral conditions.

Figure 6 Change of h with different J_p/J for cracked pipes.

Then, the normalized fully plastic J-integrals are calculated from Equation (12) after the total J-integrals and elastic J-integrals being obtained for the pipes with different crack aspect ratios, relative depth ratios, inclination angles, and material properties. The typical results of h against different crack geometries, inclination angles, and material properties are presented in Figures 7 and 8.

Figure 7 Change of normalised fully plastic J-integrals along the crack front with different strain hardening exponents for pipe d/R=0.1, a/d=0.5, a/c=1.0: (a) β=15°; (b) β=45°; (b) β=75°.

Figure 8 Change of normalised fully plastic J-integrals along the crack front with different aspect ratios for pipe d/R=0.025, a/d=0.2, a/c=0.4, n=5: (a) β=15°; (b) β=45°; (b) β=75°.

From these figures, it is found in general that all the normalized fully plastic J-integrals for inclined surface cracks in pressurized pipes are symmetric to the deepest point of the crack. It is also found that the distributions of h are different for various inclination angles (β) and aspect ratios (a/c) while they are analogous for different strain hardening exponents (n) and relative depth ratios (a/d). For given crack geometries, as seen in Figures 7a-c, increasing the strain hardening exponents (n) will increase the values of h although the general trends are similar. This can be understood since with n increasing from 3 to 10, the material tends to be more plastically deformed under the applied load. For the same extension of crack more external energy work (load) is required in material with larger n, as a result, a larger h is obtained. Also, by comparing the difference of h in Figures 7a-c, it can be found that the difference of h between different n in cracks with β=15° *and* 45° is relatively larger than that

in cracks with β=75°. This indicates that the elasto-plastic J-integral is less sensitive to the change of strain exponent in surface cracks with a high inclination angle.

For β=15°, the maximum value of h is found at ξ=±0.25 as seen in Figure 7a. This means that the critical locations for crack propagation are between the surface point and the deepest point of cracks with relatively small inclination angles. As a result, its original semi-elliptical geometry can be altered to irregular one during the process of crack growth. A similar result was observed Yagawa et al. (1993) who determined the fully plastic J-integral for the semi-elliptical surface cracked plates subjected to uniform tension by use of the virtual crack extension method. When β=45° (except for n=10) and 75°, the maximum values of h, however, are found at the surface point (ξ=±0.1) for crack with a/c=1.0, as shown in Figures 7b-c. This means that cracks with relatively large inclination angles tend to extend its length after excessive loading. The same can be found as the change of stress intensity factors, as observed by many researchers, e.g., Li et al. 2016, Wang et al. 2017, Raju and Newman 1979,1982, etc.

Also, it can be seen from Figure 7 that with the inclination angle increasing from 15° to 75°, the magnitude of h generally decreases. This can be understood because the increase of the inclination angle can cause a decrease of the hoop stress component that is normal to the crack surface. This indicates that the pipes with a small inclination angle are easier to fracture under internal pressure which needs more attention. For other values of relative depth ratios and wall thickness to inner radius ratios, similar trends are observed and the figures can be produced similarly but are omitted here.

To reveal the effect of crack aspect ratios (a/c) together with different inclination angles on J_p, the changes of h for cracked pipes with d/R=0.025, a/d=0.2, a/c=0.4, n=5 are presented in Figures 8a-c. From the results, it can be seen that for given inclination angles, the critical

328 locations for crack propagation varies from low aspect ratio (a/c=0.4) to high aspect ratio ($a/$
329 c=1.5). Specifically, in cracks of a/c=0.4, the maximum value of h occurs at the deepest point
330 of crack for β=15°, however, it occurs at ξ=±0.25 for β= 45° and 75°. In comparison, the
331 locations of maximum h in cracks of a/c=1.0 and 1.5 are constant, i.e., at the surface point,
332 for all inclination angles. A summary of the above results suggests that h increases with the
333 decrease of crack inclination angle and aspect ratios and while with the increase of strain
334 hardening exponent.

335 The derived normalized fully plastic J-integrals at different locations along the cracks in this
336 study are tabulated in Tables 1-3, which are calculated from the results that the average
337 difference of h between d/R=0.025 and d/R=0.1 can be 8.3%, 10.1% and 14.3% for cracked
338 pipes with materials of n=3, 5 and 10, respectively. This confirms that applying the J-integral
339 solutions of thick-wall pipes to the thin-wall pipes can lead to inaccurate results (Cho et al.
340 2011, Battelle 2002). Also, it can be seen from the results that an increase of n can increase
341 the difference of h between pipes of d/R=0.025 and d/R=0.1. The above results can justify the
342 necessity of deriving h values for cracked pipes with a wide range of geometries (d/R, a/c and
343 a/d), inclination angles, and material properties, as this paper has done here.

344 **Table 1** Normalized fully plastic J-integral h for cracked pipes with n=3

345

346 **Table 2** Normalized fully plastic J-integral h for cracked pipes with n=5

347

348 **Table 3** Normalized fully plastic J-integral h for cracked pipes with n=10

349

350 The derived normalized fully plastic J-integrals can be used to calculate the total elasto-
351 plastic J-integral by adding up the elastic and fully plastic J-integrals with Equation (7) for

the complete range of elasto-plastic deformation and commonly used material properties (n =3~10). The elastic J-integrals can be determined through the equivalent influence coefficients which are published in Li et al. (2016). The fully plastic J-integral can be directly calculated through Equation (11) for various material properties, geometries of cracks and pipes. As the current pipeline systems in petroleum and water industries consist of not only old thick-wall pipes but also newly manufactured thin-wall pipes, the results presented in Tables 1-3 can be used for other required geometries and materials through appropriate interpolation or extrapolation. The elasto-plastic J-integral then can be used for accurate integrity assessment of pressurized ductile iron and steel pipes subject to inclined surface cracks.

MODELS FOR NORMALIZED FULLY PLASTIC *J*-INTEGRAL

For practical application, a predictive model of normalized fully plastic J-integral (h) is highly desirable to determine the elasto-plastic J-integral of ductile iron and steel pipes subject to inclined surface cracks. The data as presented in Tables 1-3 can be used for developing such a predictive model. In current study, a hybrid data-mining modeling technique, named Evolutionary Polynomial Regression (EPR) is employed to construct the nonlinear relationship between h and geometric and material parameters of pipes subject to inclined surface cracks. In general, the EPR constructs symbolic models by genetic algorithm (GA) at the initial stage and estimates the constant values by the least-squares method at the final stage (Giustolisi and Savic 2009). The main advantage of the EPR is that it not only returns regression models with the reasonably accurate prediction of the results but also allows for a scientific understanding of some underlying mechanisms (Wang et al. 2017, Giustolisi and Savic 2006). The version of EPR used here, i.e., EPR MOGA-XL v.1,

implements an evolutionary multi-objective genetic algorithm (MOGA) as an optimization strategy based on Pareto dominance criteria (Giustolisi and Savic 2009).

A general model of EPR can be expressed as follows (Fiore et al. 2012)

$$Y = a_o + \sum_{j=1}^{m} a_j \cdot \left(X_1\right)^{ES(j,1)} \cdot \ldots \cdot \left(X_k\right)^{ES(j,k)} \cdot f\left(\left(X_1\right)^{ES(j,k+1)} \cdot \ldots \cdot \left(X_k\right)^{ES(j,2k)}\right) \quad (13)$$

where **Y** is the estimated output matrix of the system, m is the number of additive terms, a_j are constants to be estimated, $\boldsymbol{X}_i$ is input vector of variables, k is the number of independent variables as predictors. **ES**(j,z) (with z = 1,..., 2k) is the exponent set of the z^{th} input within the j^{th} term in Equation (13), f is the inner function. In brief, the search for a model structure is performed by exploring the combinatorial space of exponents to be assigned to each candidate input of Equation (13). The multi-objective critera i.e., (i) the maximization of model accuracy, (ii) the minimization of the number of model coefficients and (iii) the minimization of the number of actually used model inputs, are used to trade off the parsimony of model against its accuracy.

Firstly, the relationship between h and other independent predictor variables, i.e., d/R, a/d, a/c, n, $\beta$and $\xi$is constructed. In total, 972 data points from 162 data set are used for model construction as shown in Tables 1-3. Based on prior knowledge of the phenomenon (Wang et al. 2017), the exponential inner function is selected. The candidate-exponents set and genetic algorithm parameters are properly chosen according to Fiore et al. (2012). After EPR runs, a set of optimal formulas by use of different model structures (including that shown in Equation13) are obtained with different accuracy, the number of terms and predictor variables. Among all the formulas, two of them are selected as follows:

$$h = a_o + \sqrt[3]{\frac{c}{d}}\sqrt{\frac{d}{R}}(\cos\beta)^2 a_1 \exp\left(\sqrt[3]{\frac{a}{d}}\sqrt{n}\cos\beta\right) + \sqrt[3]{\xi}\sqrt{\frac{a}{R}\cos\beta}\, n\left(\frac{c}{a}\right)^2 a_2 \exp\left[\sqrt{\frac{a}{d}}\left(\frac{c}{a}\right)^2 \xi^2 \cos\right. \quad (14a)$$

$$h = a_o + \sqrt[3]{\frac{a\cos\beta}{d}}\sqrt{\frac{Rn}{d}}\,a_1 \exp\left[\sqrt{\xi}\left(\frac{a}{d}\right)^2\right] + \frac{an}{d}\xi^2\sqrt{\frac{d}{R}}\,a_2 \exp\left[\xi^2\cos\beta\sqrt{\frac{a}{d}}\left(\frac{c}{a}\right)^2\right] + \sqrt{\frac{d}{R}}\left(\frac{c\cos\beta}{d}\right) \quad (14b)$$

The range of parameters which ensures the validity of Equations (14a) and (14b) is $0.025 \le d/R \le 0.1$, $0.2 \le a/d \le 0.8$, $0.4 \le a/c \le 1.5$, $3 \le n \le 10$, $0 \le \xi \le 1$. The above formulas represent the highly nonlinear relationship between h and all other variables, including the geometries of pipe and crack, the inclination angle of crack, and the location of points along the crack front. The estimated constants and the indicators of fitting of the above models are presented in Table 4. The fit of the equations is examined by the coefficient of determination (CoD), i.e. CoD = 1−SSE/SST with CoD = 1 being a perfectly fitting model where SSE is the sum of squares of residuals, which represents the unexplained part of variance and SST is total sum of squares. The sum of squared residuals (SSE) is used to guide the search for the best-fit model. It can be seen that Equation (14a) has two terms and three constants (a_o, a_1, a_2) with CoD of 95.77% while Equation (14b) increased its fitting accuracy further (CoD=97.42%) with an increase of complexity in the model structure. Nevertheless, the indicators of fitting in both Equation (14a) and (14b) justify the efficiency of the EPR considering a large number of predictor variables and the highly complicated relationship between them.

Table 4 Constants in Equations (14) & (15) and the fitting indicators

For some applications, e.g., the structural reliability assessment of cracked pipes, the maximum *J*-integral for a given cracked pipe is most of interest to the assessors. To develop the formula of maximum h as a function of geometric and material properties of cracked pipes, further EPR is performed on 156 data points from the 162 data set. Based on the maximum h values obtained from the parametric FE simulations, two formulas with the different number of model terms are presented:

$$h = a_o + a_1 n \frac{c}{a}\sqrt{\frac{d}{R}}\left(\frac{a}{d}\cos\beta\right)^2 \exp\left[\sqrt[3]{\cos\beta}\sqrt{\frac{c}{a}}\left(\frac{a}{d}\right)^2\right] \quad (15a)$$

$$h = a_o + \frac{a_1}{\sqrt{n}}\left(\frac{d}{a}\right)^2 \sqrt[3]{\cos\beta}\exp\left(\sqrt[3]{\frac{a}{d}}\sqrt{\frac{R}{d}}\right) + a_2 n\sqrt{\frac{dc}{Ra}}\left(\frac{a}{d}\cos\beta\right)^2 \exp\left[\cos\beta\frac{c}{a}\left(\frac{a}{d}\right)^2\right] \quad (15b)$$

The valid range of parameters in the above equations is the same as that of Equation (14). The estimated constants and the indicators of fitting accuracy are also presented in Table 4. In comparison, Equations (15a) and (15b) are more parsimonious, with only one and two terms, respectively. Also, a higher level of model accuracy (CoD=97.21% and 99.02%) for the is obtained for the formulas of the maximum h. This can be easily understood since the location parameter (ξ) is deselected in the above equations, which reduces the complexity of the model structure.

It is important to verify/test the developed formulas before their application. To do this, 80 data points which were not used in the model construction are used to compare with the results predicted by Equations (14a) and (14b). The comparison result is shown in Figure 9a. It is noted that both formulas generally agree well with the whole set of data with a CoD of 93.93% and 97.70% for Equation (14a) and Equation (14b), respectively. This result confirms that Equation (14b) can predict the h values slightly better than Equation (14a). Similarly, 6 data points which were not used in the construction of Equation 15 are used to illustrate how well the developed Equation (15) can predict the maximum fully plastic J-integrals along an inclined surface crack. The comparison result is shown in Figure 9b. It can be seen that good agreements between results predicted by Equation (15a) and (15b) and test data are obtained with a CoD of 93.76 and 98.23%, respectively. It can be concluded that the developed formulas accurately predict the normalized fully plastic J-integrals for pressurized ductile iron and steel pipes subject to inclined surface cracks.

Figure 9 Comparison of results predicted by the developed formulas and testing data for (a) Equation (14) and (b) Equation (15).

CONCLUSIONS

In this paper, new solutions to fully plastic *J*-integrals for pressurized ductile pipes have been derived based on detailed three-dimensional finite element (FE) analyses. A meshing technique with mixed types of the quadratic tetrahedron and hexahedron elements has been employed with different strain singularities to enhance the accuracy of both the elastic and total *J*-integrals. A new criterion for extracting the plastic *J*-integral with the applied load corresponding to $J_p/J=¿98\%$ has been proposed. After verification of the FE models, the effects of crack geometries, crack inclination angles, pipe dimensions and materials properties on $J_p$have been thoroughly investigated. Also, predictive models have been developed for both the maximum normalized fully plastic *J*-integrals and the values associated with specific locations along the crack front. It has been found in the paper that the normalized fully plastic *J*-integral generally increases with the decrease of crack inclination angle and aspect ratios and the increase of strain hardening exponent and that a considerable difference exists in the normalized fully plastic *J*-integral between thick-wall and thin-wall pipes. It has also been found that the critical locations of crack propagation generally occur between the surface point and the deepest point of the crack when the inclination angle is 15^{o} for all cases except for the low aspect ratio (a/c=0.4) with large strain hardening exponent (n=10). It can be concluded that the *J*-integrals for inclined surface cracks highly relies on the geometries and pipe materials, and the developed formulas can accurately predict the elasto-plastic *J*-integrals for inclined surface cracks. The results presented in the paper can enable researchers and practitioners to accurately predict the mixed-mode fracture failure of pressurized ductile pipes subjected to inclined surface cracks.

ACKNOWLEDGEMENT

Financial support from the Australian Research Council under DP140101547, LP150100413 and DP170102211, and the National Natural Science Foundation of China with Grant No. 51820105014 is gratefully acknowledged.

REFERENCE

Abaqus, V. (2014). 6.14 Documentation. Dassault Systemes Simulia Corporation, 651.

Aliha, M. R. M., and Ayatollahi, M. R. (2007). A fracture mechanics approach for analysing spiral weld pipes containing crack. In First Iranian Pipe and Pipeline Conference, Tehran, Iran.

Anderson, T. L. (2005) Fracture mechanics: fundamentals and applications. Boca Raton, Fla.: Taylor & Francis.

Aristizabal, R., Druschitz, A., Druschitz, E., Bragg, R., Hubbard, C. R., Watkins, T. R., and Ostrander, M. (2011). Intercritically austempered ductile iron. Oak Ridge National Lab. (ORNL), Oak Ridge, TN (United States); High Flux Isotope Reactor; High Temperature Materials Laboratory.

Ayhan, A. O. (2004). Mixed mode stress intensity factors for deflected and inclined surface cracks in finite-thickness plates. Engineering fracture mechanics, 71(7-8), 1059-1079.

Barsoum, R. S. (1975). Further application of quadratic isoparametric finite elements to linear fracture mechanics of plate bending and general shells. International Journal of Fracture, 11(1), 167-169.

Battelle. (2002) Development of Flaw Evaluation Criteria for Class 2, 3 and Balance of Plant Piping, NUREG/CR-6837.

Cho, D. H., Seo, H. B., Kim, Y. J., Chang, Y. S., Jhung, M. J., and Choi, Y. H. (2011). Advances in J−integral estimation of circumferentially surface cracked pipes. Fatigue & Fracture of Engineering Materials & Structures, 34(9), 667-681.

Conlin, R. M., and Baker, T. J. (1991). Application of fracture mechanics to the failure behaviour of buried cast iron mains. Contractor Report-Department of Transport Transport and Road Research Laboratory.

Fiore, A., Berardi, L., and Marano, G. C. (2012). Predicting torsional strength of RC beams by using evolutionary polynomial regression. Advances in Engineering Software, 47(1), 178-187.

Fu, G., Yang, W., and Li, C. Q. (2017). Elasto and fully plastic J-integrals for mixed mode fracture induced by inclined surface cracks in plates under biaxial loading. Engineering Fracture Mechanics, 186, 483-495.

Jayadevan, K. R., Østby, E., and Thaulow, C. (2004). Fracture response of pipelines subjected to large plastic deformation under tension. International Journal of Pressure Vessels and Piping, 81(9), 771-783.

Kim, Y. J., Kim, J. S., Park, Y. J., and Kim, Y. J. (2004). Elastic–plastic fracture mechanics method for finite internal axial surface cracks in cylinders. Engineering Fracture Mechanics, 71(7-8), 925-944.

Kumar, V. G. M. D., German, M. D., and Shih, C. F. (1981). Engineering approach for elasto-plastic fracture analysis (No. EPRI-NP--1931). General Electric Co..

506 Kumar, V. A. G. M., and German, M. D. (1988). Elasto-plastic fracture analysis of through-
507 wall and surface flaws in cylinders (No. EPRI-NP-5596). General Electric Co.,
508 Schenectady, NY (USA). Corporate Research and Development Center.

509 Lei, Y. (2004). J-integral and limit load analysis of semi-elliptical surface cracks in plates
510 under combined tension and bending. International journal of pressure vessels and
511 piping, 81(1), 43-56.

512 Li, C. Q., and Yang, S. T. (2012). Stress intensity factors for high aspect ratio semi-elliptical
513 internal surface cracks in pipes. International Journal of Pressure Vessels and Piping,
514 96, 13-23.

515 Li, C. Q., Fu, G., and Yang, W. (2016). Stress intensity factors for inclined external surface
516 cracks in pressurised pipes. Engineering Fracture Mechanics, 165, 72-86.

517 Liu, X., Lu, Z. X., Chen, Y., Sui, Y. L., and Dai, L. H. (2018). Failure Assessment for the
518 High-Strength Pipelines with Constant-Depth Circumferential Surface Cracks.
519 Advances in Materials Science and Engineering, 2018.

520 Gamboa, E., Linton, V., and Law, M. (2008). Fatigue of stress corrosion cracks in X65
521 pipeline steels. International journal of fatigue, 30(5), 850-860.

522 Giustolisi, O., and Savic, D. A. (2009). Advances in data-driven analyses and modelling
523 using EPR-MOGA. Journal of Hydroinformatics, 11(3-4), 225-236.

524 Giustolisi, O., and Savic, D. A. (2006). A symbolic data-driven technique based on
525 evolutionary polynomial regression. Journal of Hydroinformatics, 8(3), 207-222.

526 Makar, J. M., Desnoyers, R., and McDonald, S. E. (2001). Failure modes and mechanisms in
527 gray cast iron pipe. Underground Infrastructure Research, 1-10.

528 Moghaddam, A. S., Alfano, M., and Ghajar, R. (2013). Determining the mixed mode stress
529 intensity factors of surface cracks in functionally graded hollow cylinders. Materials &
530 Design, 43, 475-484.

531 National Research Council. (2006). Drinking water distribution systems: assessing and
532 reducing risks. National Academies Press.

533 Newman Jr, J. C., & Raju, I. S. (1981). An empirical stress-intensity factor equation for the
534 surface crack. Engineering fracture echanics, 15(1-2), 185-192.

535 Nikishkov, G. P., and Atluri, S. N. (1987). Calculation of fracture mechanics parameters for
536 an arbitrary three−dimensional crack, by the 'equivalent domain integral'method.
537 International journal for numerical methods in engineering, 24(9), 1801-1821.

538 Østby, E., Jayadevan, K. R., and Thaulow, C. (2005). Fracture response of pipelines subject
539 to large plastic deformation under bending. International Journal of Pressure Vessels
540 and Piping, 82(3), 201-215.

541 Parks, D. M., and White, C. S. (1982). Elasto-plastic line-spring finite elements for surface-
542 cracked plates and shells. Journal of Pressure Vessel Technology, 104(4), 287-292.

543 Raju, I. S., and Newman Jr, J. C. (1982). Stress-Intensity Factor Influence Coefficients for
544 Internal and External Surface Cracks in Cylindrical Vessels. Aspects of fracture
545 mechanics in pressure vessels and piping, 37-49.

546 Raju, I. S., and Newman Jr, J. C. (1979). Stress-intensity factors for a wide range of semi-
547 elliptical surface cracks in finite-thickness plates. Engineering fracture mechanics,
548 11(4), 817-829.

549 Rice JR and Rosengren GF. Plane strain deformation near a crack tip in a power-law
550 hardening material. J Mech Phys Solids 1968;16:1–12

551 Sih, G. C., and Lee, Y. D. (1989). Review of triaxial crack border stress and energy behavior.
552 Theoretical and Applied Fracture Mechanics, 12(1), 1-17.

553 Shlyannikov, V. N. (2013). Elastic-plastic mixed-mode fracture criteria and parameters (Vol.
554 7). Springer Science & Business Media.

555 Shahani, A. R., and Habibi, S. E. (2007). Stress intensity factors in a hollow cylinder
556 containing a circumferential semi-elliptical crack subjected to combined loading.
557 International journal of Fatigue, 29(1), 128-140.

558 Standard, A. S. T. M. (2001). Standard test method for measurement of fracture toughness.
559 ASTM, E1820-01, 1-46.

560 Wang, W., Yang, W., Li, C. Q., and Yang, S. (2020). A new method to determine elasto-
561 plastic j-integral for steel pipes with longitudinal semi-elliptical surface cracks.
562 Engineering Failure Analysis, 118, 104915.

563 Wang, W., Zhou, A., Fu, G., Li, C. Q., Robert, D., and Mahmoodian, M. (2017). Evaluation
564 of stress intensity factor for cast iron pipes with sharp corrosion pits. Engineering
565 Failure Analysis, 81, 254-269.

566 Wang, X. (2006). Fully plastic J-integral solutions for surface cracked plates under biaxial
567 loading. Engineering fracture mechanics, 73(11), 1581-1595.

568 Yagawa G, Kitajima Y and Ueda H (1993). Three-dimensional fully plastic solutions for
569 semielliptical surface cracks. Int J Pressures Vessel Piping, 53: 457–510

570 Zadow, L., Gamboa, E., and Lavigne, O. (2015). Inclined stress corrosion cracks in gas
571 pipeline steels: morphology and implications. Materials and Corrosion, 66(10), 1092-
572 1100.

573 LIST OF TABLES
574

575 1. Normalized fully plastic *J*-integral *h* for cracked pipes with *n*=3.
576 2. Normalized fully plastic *J*-integral *h* for cracked pipes with *n*=5.
577 3. Normalized fully plastic *J*-integral *h* for cracked pipes with *n*=10.
578 4. Constants in Equations (14) & (15) and the fitting indicators.

Table 1 Normalized fully plastic J-integral h for cracked pipes with n=3.

d/R=0.025										
ξ	a/d	a/c=0.4			a/c=1.0			a/c=1.5		
		β=15°	β=45°	β=75°	β= 15°	β= 45°	β=75°	β= 15°	β= 45°	β=75°
1	0.2	1.26	1.93	0.32	1.68	2.08	0.47	1.41	1.51	0.37
0.8		2.76	1.50	0.16	2.56	1.29	0.19	1.94	1.13	0.15
0.6		3.63	1.87	0.22	2.51	1.25	0.18	1.46	1.05	0.14
0.4		4.17	2.14	0.26	2.41	1.19	0.18	1.45	0.90	0.12
0.2		4.47	2.29	0.29	2.33	1.12	0.18	1.94	0.72	0.09
0		4.58	2.35	0.30	2.30	1.08	0.18	1.41	0.60	0.08
1	0.5	2.86	3.85	0.62	2.97	3.13	0.82	2.54	2.53	0.60
0.8		7.25	3.13	0.30	4.59	2.38	0.28	3.73	1.97	0.24
0.6		8.81	3.96	0.42	4.37	2.25	0.26	3.36	1.78	0.22
0.4		9.65	4.60	0.50	4.11	2.08	0.26	2.87	1.52	0.19
0.2		10.28	4.86	0.55	3.89	1.94	0.25	2.36	1.20	0.15
0		10.27	4.95	0.57	3.77	1.86	0.25	2.14	0.99	0.12
1	0.8	13.97	13.13	1.68	10.32	10.65	1.91	7.36	7.85	1.85
0.8		36.61	14.03	0.82	17.55	8.08	0.78	11.88	5.81	0.65
0.6		37.33	16.08	1.12	15.40	7.38	0.74	10.37	5.11	0.59
0.4		34.07	15.98	1.44	12.92	6.46	0.75	8.34	4.29	0.53
0.2		34.73	17.66	1.88	10.67	5.96	0.74	6.41	3.31	0.41
0		34.17	17.20	2.08	10.65	5.62	0.72	5.44	2.64	0.33
d/R=0.1										
ξ	a/d	a/c=0.4			a/c=1.0			a/c=1.5		
		β=15°	β=45°	β=75°	β= 15°	β= 45°	β=75°	β= 15°	β= 45°	β=75°
1	0.2	1.15	1.84	0.31	1.51	1.97	0.45	1.40	1.52	0.34
0.8		2.59	1.58	0.19	2.30	1.34	0.17	2.06	1.16	0.13
0.6		3.40	1.96	0.26	2.28	1.29	0.16	1.90	1.07	0.11
0.4		3.90	2.22	0.30	2.22	1.22	0.16	1.66	0.92	0.06
0.2		4.17	2.36	0.33	2.17	1.13	0.16	1.41	0.73	0.04
0		4.27	2.41	0.34	2.15	1.08	0.16	1.29	0.61	0.02
1	0.5	2.88	3.15	0.44	3.24	3.31	0.75	2.40	2.88	0.73
0.8		6.85	3.50	0.34	5.06	2.60	0.30	3.95	2.09	0.26
0.6		8.98	4.31	0.46	4.82	2.46	0.28	3.56	1.89	0.23
0.4		10.67	4.99	0.55	4.54	2.27	0.27	3.01	1.60	0.20
0.2		11.07	5.32	0.62	4.26	2.08	0.27	2.43	1.23	0.15
0		11.38	5.45	0.63	4.13	2.00	0.27	2.14	1.01	0.13
1	0.8	16.51	10.49	1.22	11.77	10.27	2.14	7.98	8.43	2.01
0.8		44.78	15.41	1.00	18.97	8.64	0.85	13.33	6.44	0.71
0.6		51.99	18.03	1.31	16.85	7.55	0.80	11.55	5.70	0.64
0.4		49.91	19.22	1.68	14.13	7.03	0.79	9.18	4.68	0.57
0.2		47.39	19.26	2.10	12.15	6.22	0.77	6.97	3.58	0.43
0		45.84	19.73	2.33	10.69	5.70	0.78	5.89	2.72	0.35

583
584
585 **Table 2** Normalized fully plastic *J*-integral *h* for cracked pipes with *n*=5.

d/*R*=0.025										
ξ	*a*/*d*	*a*/*c*=0.4			*a*/*c*=1.0			*a*/*c*=1.5		
		β=15°	β=45°	β=75°	β= 15°	β= 45°	β=75°	β= 15°	β= 45°	β=75°
1	0.2	1.38	2.06	0.34	1.67	1.96	0.51	1.36	1.46	0.41
0.8		3.44	1.76	0.18	2.92	1.47	0.21	2.20	1.28	0.16
0.6		4.54	2.20	0.26	2.94	1.45	0.20	2.11	1.21	0.15
0.4		5.22	2.51	0.32	2.82	1.40	0.21	1.87	1.05	0.14
0.2		5.59	2.69	0.36	2.71	1.33	0.22	1.62	0.86	0.11
0		5.79	2.78	0.37	2.68	1.28	0.22	1.47	0.70	0.09
1	0.5	3.08	4.33	0.62	3.06	3.15	0.85	2.58	2.49	0.65
0.8		9.06	4.11	0.32	5.46	2.76	0.30	4.31	2.25	0.27
0.6		11.37	5.06	0.47	5.38	2.67	0.29	4.05	2.08	0.25
0.4		12.73	5.86	0.58	5.05	2.46	0.30	3.51	1.81	0.22
0.2		12.06	6.28	0.64	4.77	2.32	0.30	2.84	1.44	0.18
0		12.27	6.34	0.68	4.57	2.21	0.31	2.59	1.19	0.15
1	0.8	14.74	14.22	1.82	11.36	11.17	2.08	7.88	7.88	1.98
0.8		45.91	16.76	1.03	22.70	10.09	0.86	14.73	7.06	0.74
0.6		45.01	18.42	1.58	20.62	9.49	0.84	13.53	6.38	0.67
0.4		41.54	18.58	2.23	17.06	8.38	0.90	10.98	5.38	0.62
0.2		42.79	19.29	2.62	13.81	7.82	0.92	8.28	4.23	0.51
0		41.68	18.73	2.68	14.23	7.47	0.91	7.02	3.38	0.42
d/*R*=0.1										
ξ	*a*/*d*	*a*/*c*=0.4			*a*/*c*=1.0			*a*/*c*=1.5		
		β=15°	β=45°	β=75°	β= 15°	β= 45°	β=75°	β= 15°	β= 45°	β=75°
1	0.2	1.17	2.02	0.33	1.51	1.97	0.51	1.45	1.54	0.43
0.8		2.98	1.85	0.20	2.54	1.53	0.19	2.37	1.36	0.17
0.6		3.92	2.27	0.28	2.61	1.48	0.18	2.28	1.28	0.16
0.4		4.48	2.57	0.35	2.57	1.39	0.18	2.02	1.11	0.14
0.2		4.75	2.73	0.39	2.50	1.28	0.19	1.73	0.89	0.11
0		4.87	2.79	0.40	2.47	1.23	0.19	1.59	0.74	0.09
1	0.5	3.54	4.13	0.48	3.43	3.49	0.83	2.50	2.89	0.82
0.8		11.78	4.73	0.36	6.20	3.11	0.33	4.60	2.45	0.29
0.6		14.30	5.96	0.51	6.03	3.00	0.31	4.33	2.24	0.26
0.4		15.82	6.81	0.64	5.75	2.76	0.32	3.68	1.91	0.23
0.2		16.01	7.28	0.73	5.32	2.52	0.33	2.92	1.46	0.18
0		16.33	7.54	0.75	5.11	2.39	0.33	2.52	1.20	0.15
1	0.8	21.14	13.66	1.38	13.00	7.20	1.56	8.92	8.96	2.27
0.8		68.43	21.79	1.11	16.18	7.13	0.63	17.07	8.12	0.82
0.6		77.95	25.14	1.49	14.95	6.14	0.60	15.50	7.21	0.75
0.4		71.20	26.07	2.01	12.31	5.91	0.62	12.06	6.06	0.68
0.2		69.69	25.20	2.63	10.45	5.25	0.62	9.32	4.52	0.53
0		66.22	25.78	2.97	8.64	4.60	0.64	7.66	3.45	0.43

586

587
588
589 **Table 3** Normalized fully plastic *J*-integral *h* for cracked pipes with *n*=10.

d/*R*=0.025										
ξ	*a*/*d*	*a*/*c*=0.4			*a*/*c*=1.0			*a*/*c*=1.5		
		β=15°	β=45°	β=75°	β= 15°	β= 45°	β=75°	β= 15°	β= 45°	β=75°
1	0.2	1.80	2.10	0.35	1.56	1.69	0.52	1.27	1.35	0.43
0.8		5.14	2.05	0.19	3.15	1.71	0.23	2.47	1.46	0.17
0.6		6.70	2.56	0.30	3.30	1.72	0.22	2.50	1.43	0.16
0.4		7.75	2.92	0.39	3.11	1.80	0.23	2.23	1.25	0.15
0.2		8.24	3.17	0.45	3.23	1.77	0.26	1.95	1.04	0.14
0		8.48	3.24	0.48	1.56	1.63	0.52	1.27	1.35	0.43
1	0.5	4.10	4.70	0.62	2.93	3.03	0.87	2.61	2.42	0.69
0.8		14.74	5.42	0.34	5.46	2.65	0.32	5.22	2.64	0.30
0.6		17.87	6.57	0.54	9.25	4.19	0.31	5.18	2.56	0.28
0.4		19.69	7.75	0.69	4.77	2.12	0.35	4.53	2.23	0.26
0.2		18.71	8.30	0.78	6.93	3.36	0.39	3.58	1.80	0.22
0		18.28	8.42	0.83	2.93	3.03	0.40	2.61	2.42	0.69
1	0.8	21.44	16.85	1.98	12.63	11.71	2.29	9.46	8.00	2.11
0.8		79.22	23.89	1.19	32.96	13.39	0.96	22.02	9.25	0.87
0.6		73.35	24.87	1.94	31.85	13.05	0.96	21.62	8.75	0.79
0.4		67.30	24.98	2.94	25.25	11.62	1.09	17.51	7.48	0.77
0.2		71.13	28.53	3.68	20.14	11.01	1.18	13.33	5.90	0.66
0		71.30	25.61	3.76	21.78	10.64	2.29	11.25	4.72	0.55
d/*R*=0.1										
ξ	*a*/*d*	*a*/*c*=0.4			*a*/*c*=1.0			*a*/*c*=1.5		
		β=15°	β=45°	β=75°	β= 15°	β= 45°	β=75°	β= 15°	β= 45°	β=75°
1	0.2	1.30	2.26	0.38	1.64	1.99	0.59	1.41	1.47	0.51
0.8		3.86	2.37	0.23	3.24	1.94	0.23	2.73	1.56	0.20
0.6		5.04	2.90	0.35	3.43	1.90	0.22	2.76	1.54	0.19
0.4		5.76	3.32	0.44	3.41	1.79	0.24	2.43	1.28	0.17
0.2		6.05	3.57	0.50	3.30	1.69	0.26	2.08	1.10	0.15
0		6.22	3.65	0.51	1.64	1.61	0.59	1.41	1.47	0.51
1	0.5	4.45	4.75	0.56	3.98	3.93	0.99	2.66	2.91	0.93
0.8		18.03	6.10	0.43	8.68	4.19	0.41	6.01	3.19	0.36
0.6		20.88	7.58	0.62	8.94	4.19	0.38	6.03	3.00	0.32
0.4		22.31	8.38	0.84	8.46	3.81	0.42	5.09	2.55	0.29
0.2		21.83	9.04	1.02	7.94	3.56	0.44	4.00	1.96	0.24
0		22.67	8.99	1.03	3.98	3.93	0.99	3.37	1.60	0.20
1	0.8	36.49	21.09	1.75	17.79	14.45	3.07	10.81	10.18	2.70
0.8		168.07	40.92	1.41	42.36	17.81	1.33	26.15	12.16	1.08
0.6		149.93	45.33	1.96	41.29	15.73	1.28	25.37	11.13	0.97
0.4		141.85	46.86	2.79	33.50	15.27	1.41	19.23	9.38	0.93
0.2		138.25	44.76	3.88	28.48	13.75	1.46	15.34	6.92	0.74
0		135.18	44.84	4.44	17.79	14.45	3.07	12.11	5.09	0.60

590

591

592
593
594

Table 4 Constants in Equations (14) & (15) and the fitting indicators.

Equation	a_o	a_1	a_2	a_3	CoD	SSE
14a	1.3988	19.2711	-0.027253	----	95.77%	8.96
14b	0.77283	0.58134	-0.19829	10.2172	97.42%	5.46
15a	1.7132	13.3857	---	----	97.21%	9.26
15b	0.54248	0.14018	11.8319	----	99.02%	3.27

595

596 LIST OF FIGURES

597

598 1. Schematic of pipe subject to an inclined external surface crack.
599 2. R-O fitting for stress-strain curves of ductile iron (Aristizabal et al. 2011) and Australian
600 steel G350.
601 3. Finite element model of a pressurized pipe subject to an inclined surface crack.
602 4. (a) Schematic diagram and FE model for an infinite body with an inclined crack under
603 tension loading, and (b) comparison of the present finite element results with Ayhan
604 (2004).
605 5. (a) Schematic diagram and FE model for a plate with an inclined crack under biaxial
606 loading, and (b) comparison of the present finite element results with Fu et al. (2017).
607 6. Change of h with different J_p/J for cracked pipes.
608 7. Change of normalised fully plastic J-integrals along the crack front with different strain
609 hardening exponents for pipe d/R=0.1, a/d=0.5, a/c=1.0: (a) β=15°; (b) β=45°; (b) β=75°.
610 8. Change of normalised fully plastic J-integrals along the crack front with different aspect
611 ratios for pipe d/R=0.025, a/d=0.2, a/c=0.4, n=5: (a) β=15°; (b) β=45°; (b) β=75°.
612 9. Comparison of results predicted by the developed formulas and testing data for (a)
613 Equation (14) and (b) Equation (15).

614
615

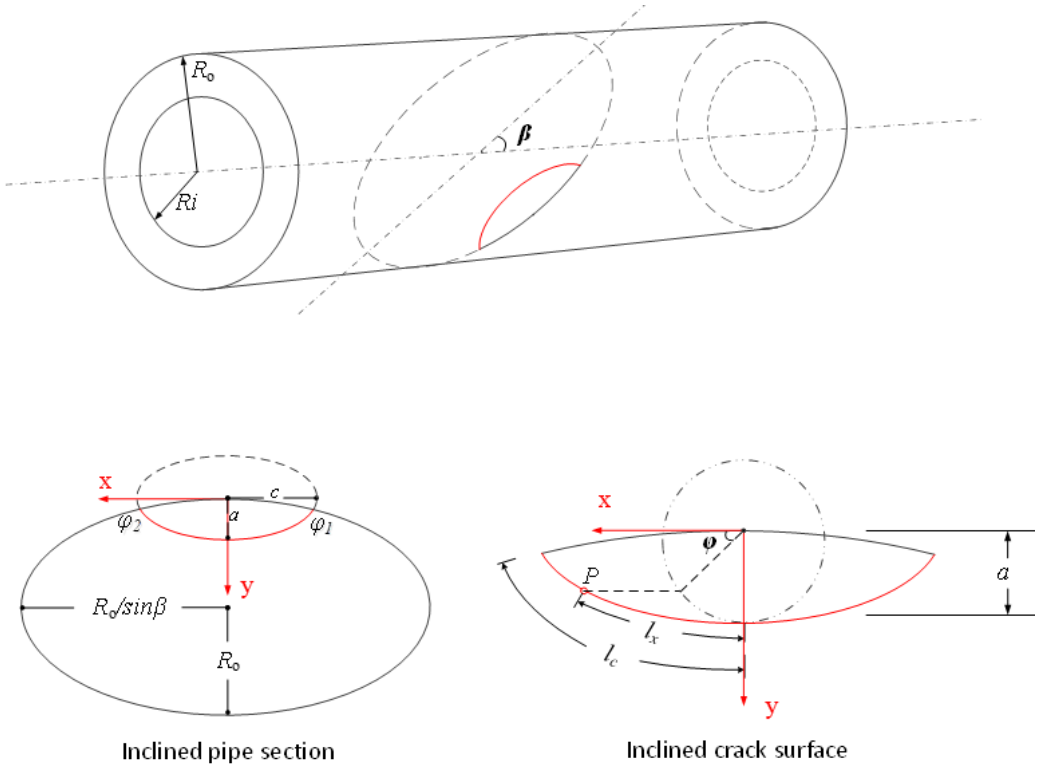

616

617 **Figure 1** Schematic of pipe subject to an inclined external surface crack.

618

619

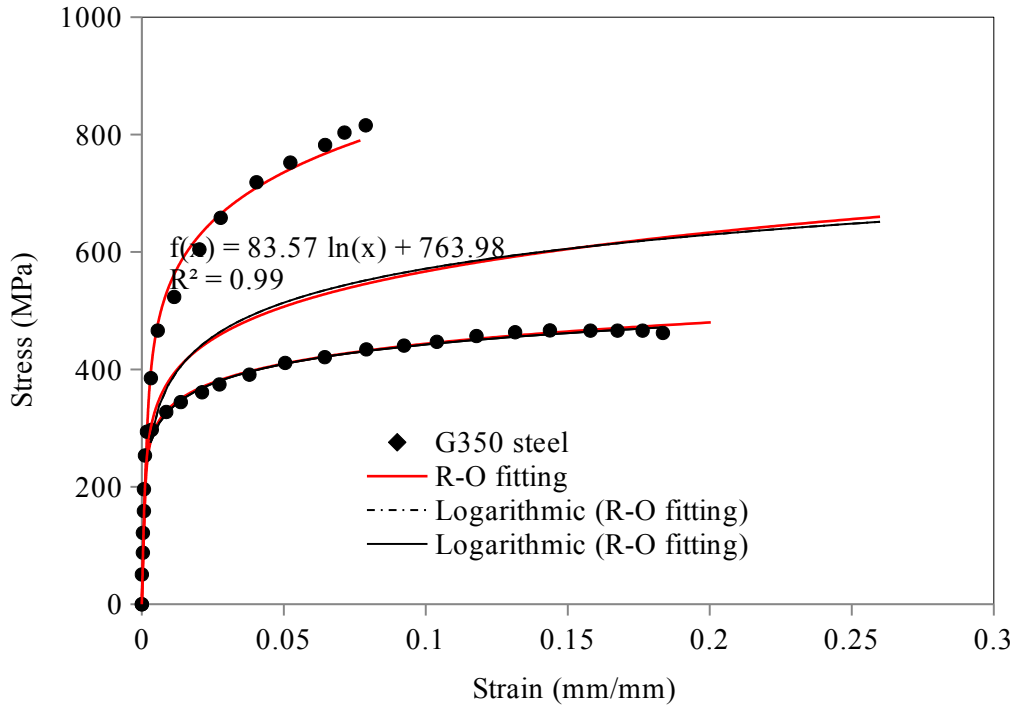

620

621 **Figure 2** R-O fitting for stress-strain curves of ductile iron (Aristizabal et al. 2011) and
622 Australian steel G350.

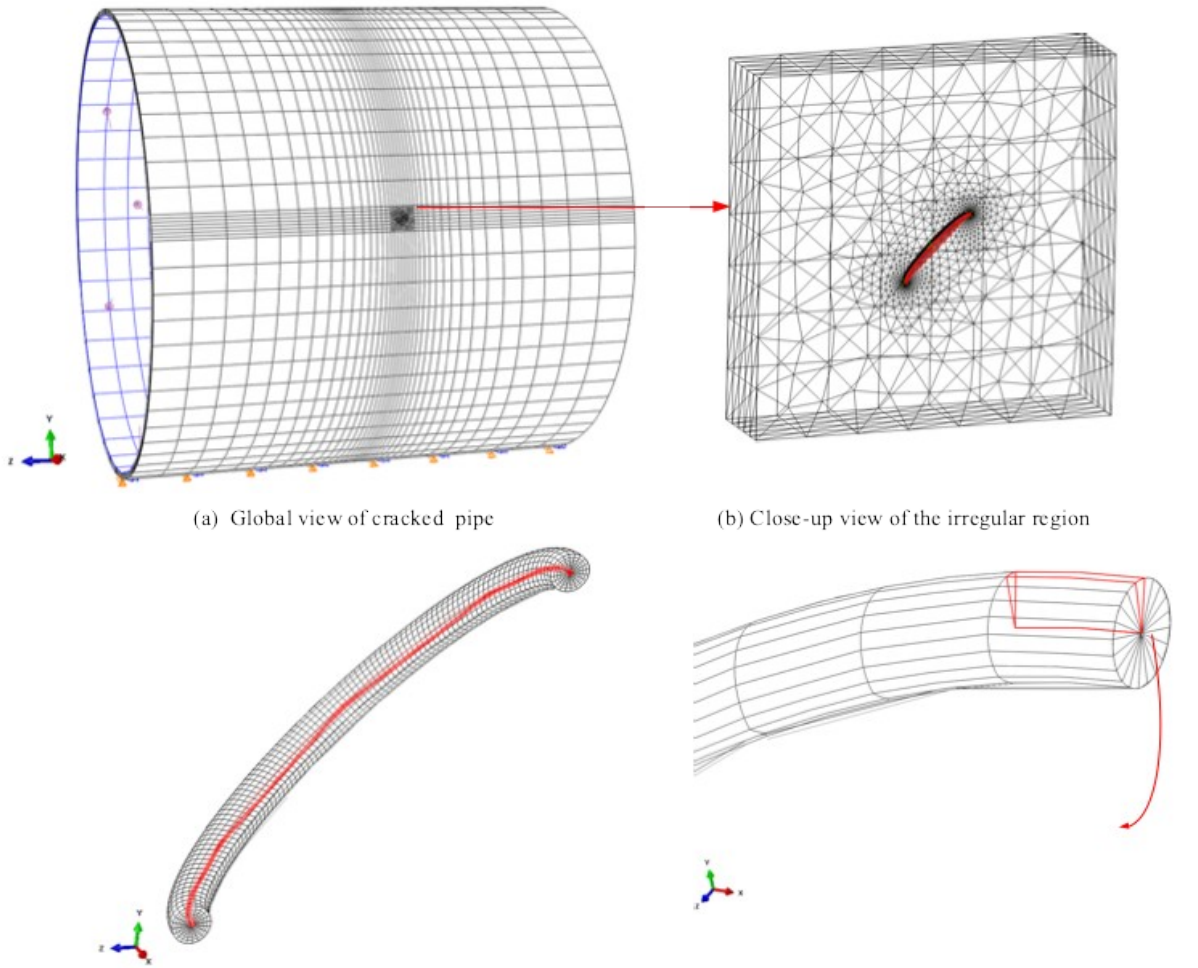

Figure 3 Finite element model of a pressurized pipe subject to an inclined surface crack.

628
629

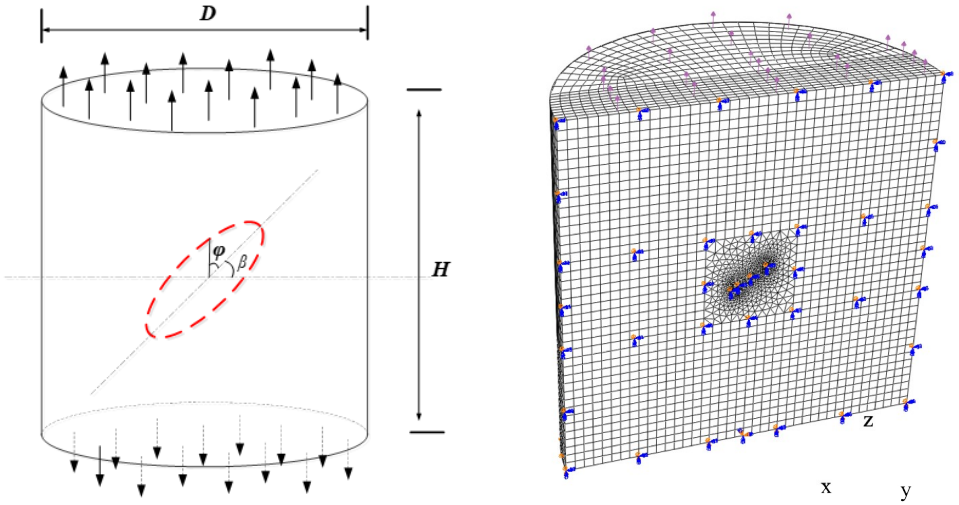

(a)

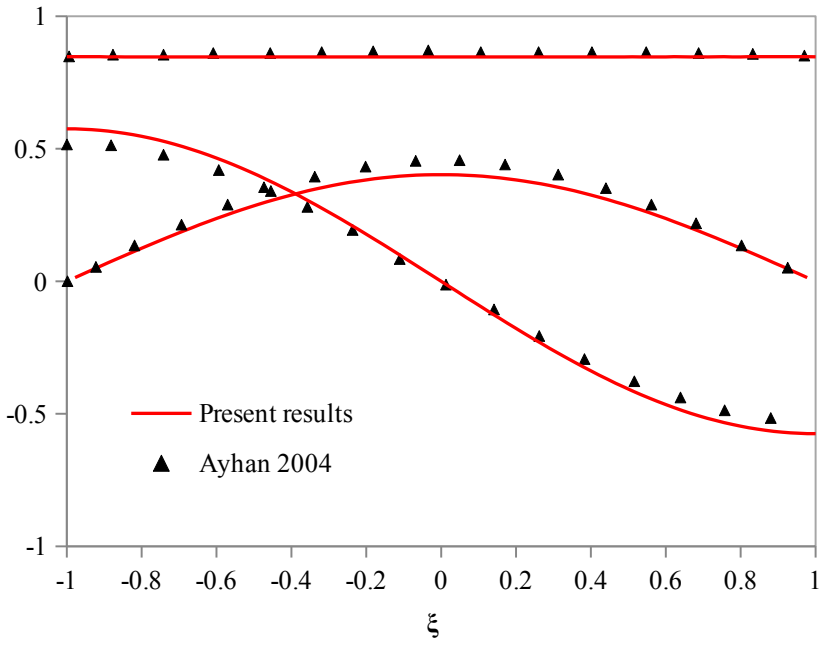

(b)

630
631

632 **Figure 4** (a) Schematic diagram and FE model for an infinite body with an inclined crack
633 under tension loading, and (b) comparison of the present finite element results with Ayhan
634 (2004).

635

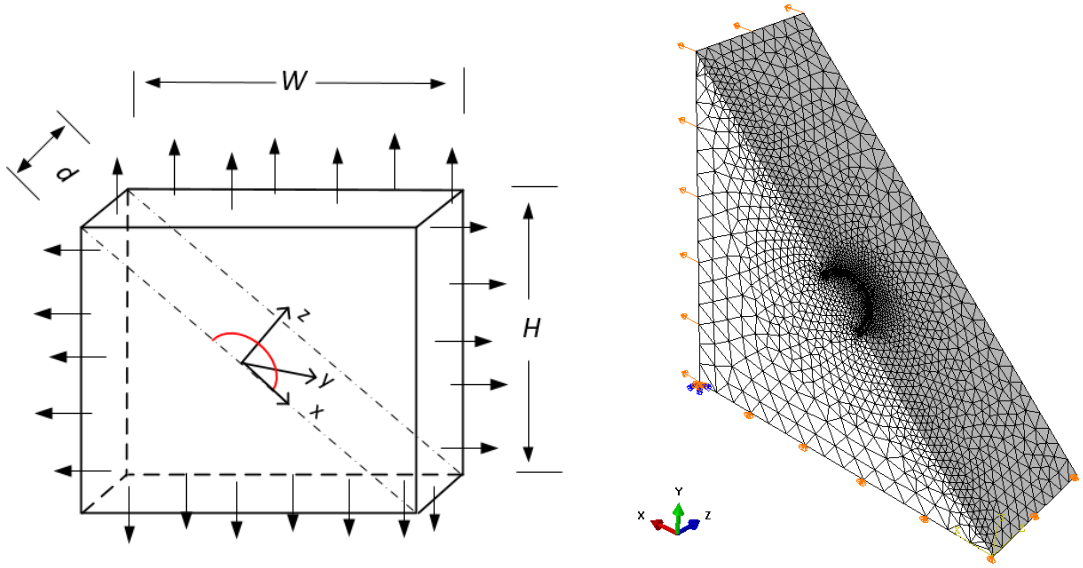

(a)

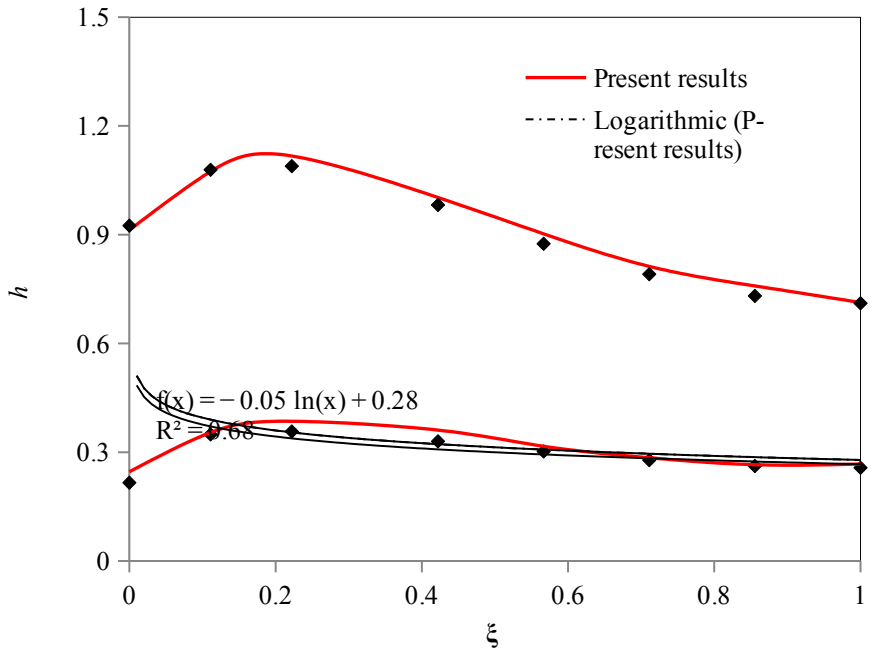

(b)

Figure 5 (a) Schematic diagram and FE model for a plate with an inclined crack under biaxial loading, and (b) comparison of the present finite element results with Fu et al. (2017).

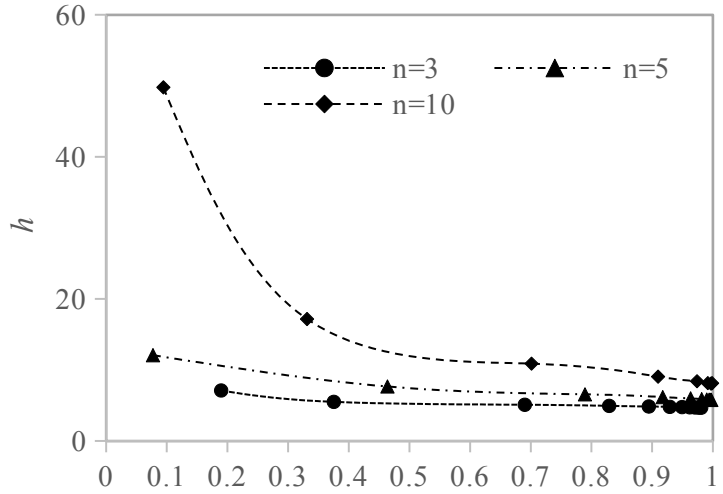

641

642 **Figure 6** Change of h with different J_p/J for cracked pipes.

643
644

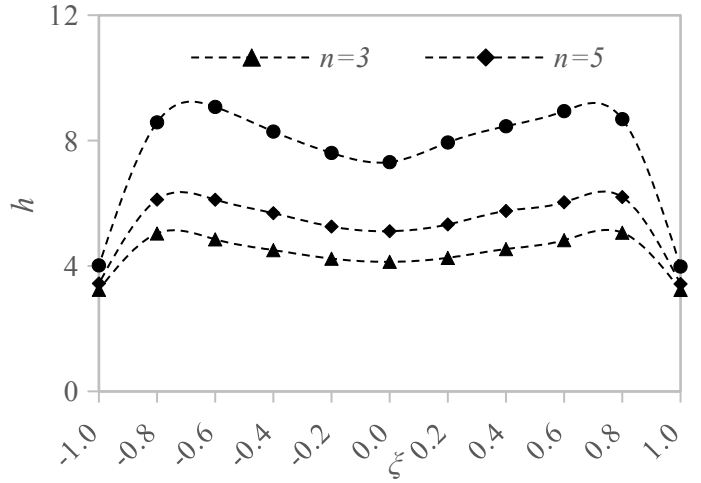

645
646

(a)

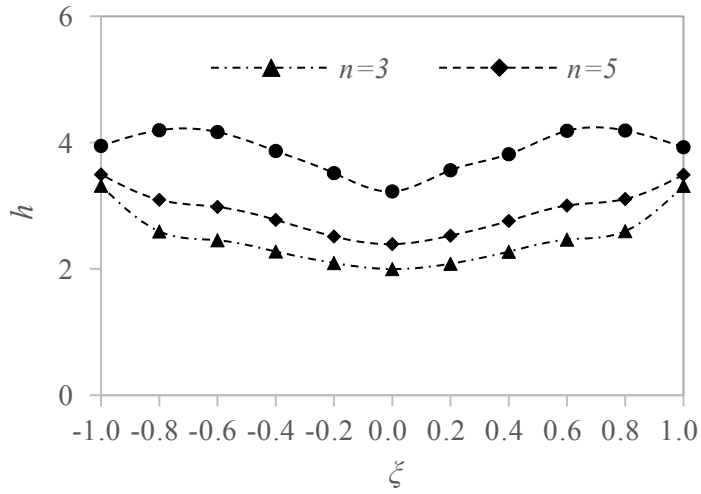

647
648

(b)

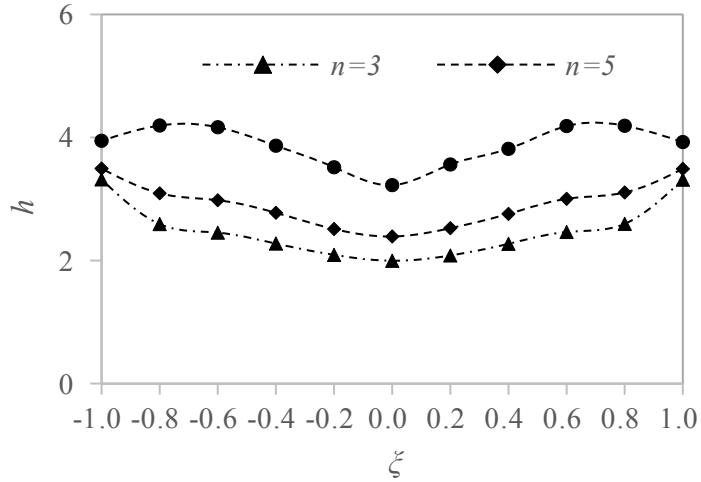

649
650

(c)

651 **Figure 7** Change of normalised fully plastic *J*-integrals along the crack front with different
652 strain hardening exponents for pipe d/R=0.1, a/d=0.5, a/c=1.0: (a) β=15°; (b) β=45°; (b)
653 β=75°.

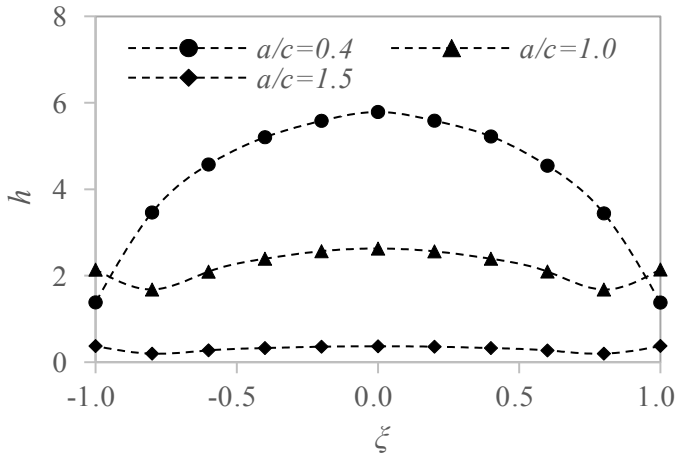

(a)

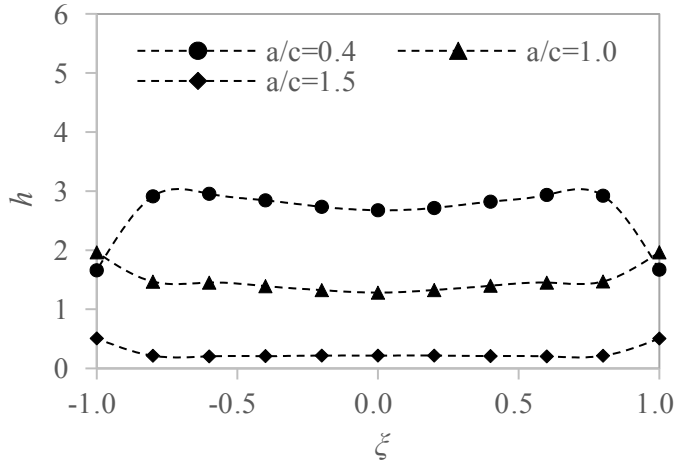

(b)

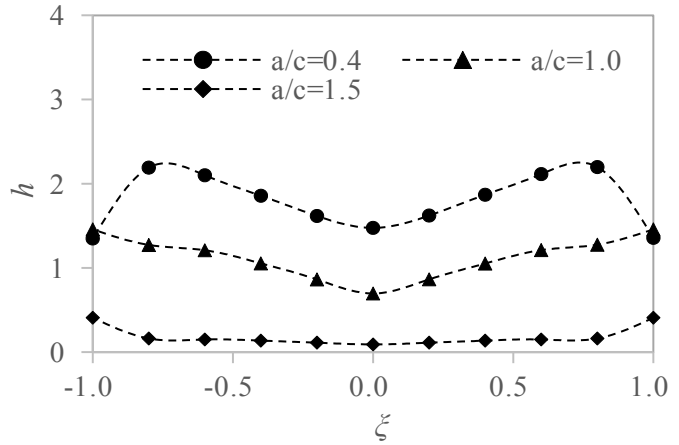

(c)

Figure 8 Change of normalised fully plastic *J*-integrals along the crack front with different aspect ratios for pipe d/R=0.025, a/d=0.2, a/c=0.4, n=5: (a) β=15°; (b) β=45°; (b) β=75°.

669
670

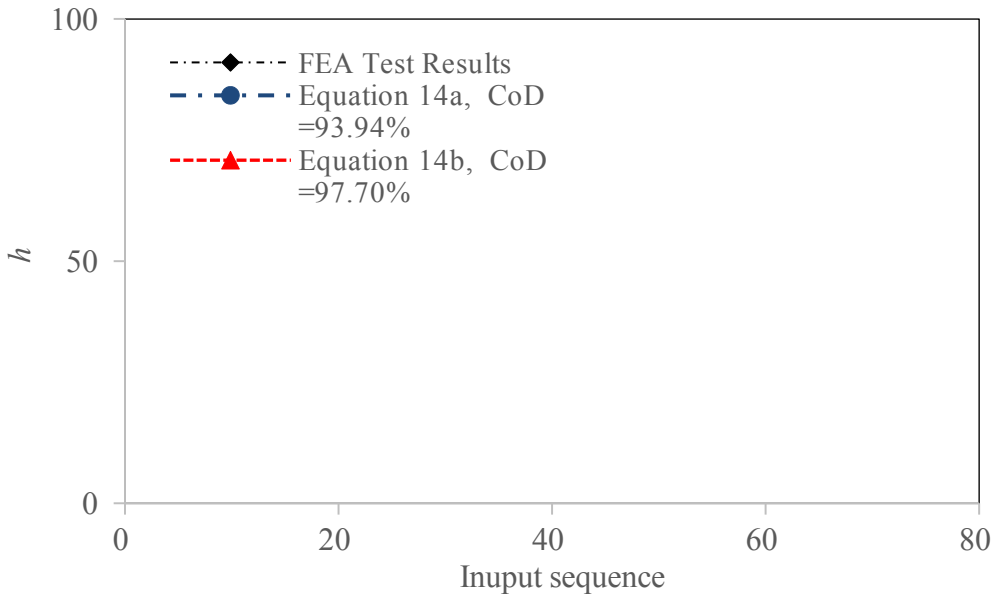

671
672

(a)

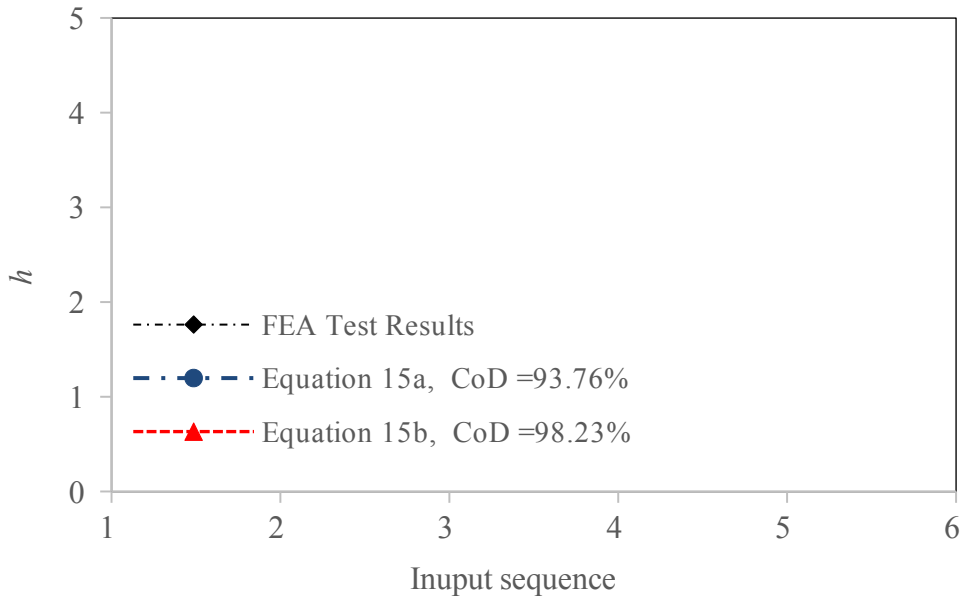

673
674

(b)

675 **Figure 9** Comparison of results predicted by the developed formulas and testing data (a) for

676 Equation (14) and (b) for Equation (15).